

Published in final edited form as:

Biochim Biophys Acta. 2013 March ; 1828(3): 981–989. doi:10.1016/j.bbame.2012.11.032.

Primary pathways of intracellular Ca²⁺ mobilization by nanosecond pulsed electric field

Iurii Semenov^{1,*}, Shu Xiao^{1,2}, and Andrei G. Pakhomov¹

¹Frank Reidy Research Center for Bioelectrics, Old Dominion University, Norfolk, VA

²Dept. of Electrical and Computer Engineering, Old Dominion University, Norfolk, VA, USA

Abstract

Permeabilization of cell membranous structures by nanosecond pulsed electric field (nsPEF) triggers transient rise of cytosolic Ca²⁺ concentration ([Ca²⁺]_i), which determines multifarious downstream effects. Using fast ratiometric Ca²⁺ imaging with Fura-2, we quantified the external Ca²⁺ uptake, compared it with Ca²⁺ release from the endoplasmic reticulum (ER), and analyzed the interplay of these processes. We utilized CHO cells which lack voltage-gated Ca²⁺ channels, so that nsPEF-induced [Ca²⁺]_i changes could be attributed primarily to electroporation. We found that a single 60-ns pulse caused fast [Ca²⁺]_i increase by Ca²⁺ influx from the outside and Ca²⁺ efflux from the ER, with the E-field thresholds of about 9 and 19 kV/cm, respectively. Above these thresholds, the amplitude of [Ca²⁺]_i response increased linearly by 8–10 nM per 1 kV/cm until a critical level between 200 and 300 nM of [Ca²⁺]_i was reached. If the critical level was reached, the nsPEF-induced Ca²⁺ signal was amplified up to 3,000 nM by engaging the physiological mechanism of Ca²⁺-induced Ca²⁺-release (CICR). The amplification was prevented by depleting Ca²⁺ from the ER store with 100 nM thapsigargin, as well as by blocking the ER inositol-1,4,5-trisphosphate receptors (IP₃R) with 50 μM of 2-aminoethoxydiphenyl borate (2-APB). Mobilization of [Ca²⁺]_i by nsPEF mimicked native Ca²⁺ signaling, but without preceding activation of plasma membrane receptors or channels. nsPEF stimulation may serve as a unique method to activate [Ca²⁺]_i and downstream cascades while bypassing the plasma membrane receptors.

Keywords

nanosecond pulses; electroporation; calcium signaling; membrane permeabilization

1. Introduction

Permeabilization of the cell plasma membrane with high-amplitude electric pulses has been known for decades and is commonly employed for intracellular delivery of xenobiotics and cell destruction [1–4]. Shortening the pulse duration into nanosecond range has the potential to permeabilize not only the plasma membrane, but the intracellular membranous structures as well [5–8]. Multiple studies have attempted to verify this theoretical prediction, with

© 2012 Elsevier B.V. All rights reserved.

*Corresponding author: Iurii Semenov, 4211 Monarch Way, Suite 318, Norfolk, VA 23508, 757-683-2234, 757-314-2397 (fax), iurii.semenov@gmail.com.

Publisher's Disclaimer: This is a PDF file of an unedited manuscript that has been accepted for publication. As a service to our customers we are providing this early version of the manuscript. The manuscript will undergo copyediting, typesetting, and review of the resulting proof before it is published in its final citable form. Please note that during the production process errors may be discovered which could affect the content, and all legal disclaimers that apply to the journal pertain.

rather diverse outcomes. Depending on the experimental approach, the studies reported only plasma membrane effects [9–13], only intracellular permeabilization [5, 14, 15], or both [16, 17].

The increase of intracellular Ca^{2+} concentration ($[\text{Ca}^{2+}]_i$) is arguably among the most consequential effects of electroporation. The resting $[\text{Ca}^{2+}]_i$ in most cell types is held tightly at about 100 nM, and its changes (increases) serve as a versatile and universal signal for activation of multifarious Ca^{2+} -dependent cascades. Depending on the cell type and physiology, as well as on the amplitude and timing of $[\text{Ca}^{2+}]_i$ transients, they may lead to such diverse effects as cell differentiation or division, cytoskeleton rearrangements, endo- and exocytosis, synthesis and release of neuromediators, activation of immune cells, apoptotic or necrotic cell death [18–24]. Elevation of $[\text{Ca}^{2+}]_i$ by nsPEF (by permeabilization of either plasma membrane or ER) is a promising approach for non-chemical triggering of Ca^{2+} -signaling in various cell types. However, experimental findings are contradictory and provide limited mechanistic analysis.

Perhaps the most detailed analysis of nsPEF effects on $[\text{Ca}^{2+}]_i$ was performed by White et al. [14]. In HL60 cells, a single 60-ns pulse at 6 or 15 kV/cm induced transient $[\text{Ca}^{2+}]_i$ increase in either Ca^{2+} -free or Ca^{2+} -containing medium. Although the latter response was much stronger, the data were interpreted as a primarily intracellular effect of nsPEF, which, in turn, could activate capacitative Ca^{2+} entry from the outside. The reason for such explanation was lack of propidium uptake by nsPEF-exposed cells, which was construed as lack of plasma membrane electroporation. However, later studies found that propidium uptake is not a reliable measure of plasma membrane permeabilization by nsPEF; instead, its “nanoelectroporation” could be efficiently revealed by electrophysiological methods, cell swelling, uptake of YO-PRO-1 dye (which is smaller than propidium), or Ti^+ entry [10, 11, 25–27]. The cell membrane remains leaky to small solutes and water for minutes after nsPEF treatment, hence Ca^{2+} entry through nanoporated plasma membrane appears a simple and logical explanation to what was originally thought as nsPEF-induced capacitative Ca^{2+} entry.

In adrenal chromaffin cells, a single 4-ns pulse at 80 kV/cm activated Ca^{2+} entry through L-type voltage sensitive Ca^{2+} channels [28]. There was no evidence of the plasma membrane electroporation unless the pulse count was increased to 50 (as detected by YO-PRO-1 uptake), and there was no response in the absence of the external Ca^{2+} . In a continuation study, a single 5-ns pulse at 50–60 kV/cm readily evoked $[\text{Ca}^{2+}]_i$ transients in a Ca^{2+} containing medium, but even a train of 10 pulses had no effect in the absence of external Ca^{2+} [29]. In cardiac myocytes, stimulation by 4-ns pulses (up to 80 kV/cm) produced rather complex effects, including formation of nanopores, opening of voltage-gated Na^+ and Ca^{2+} ion channels, and Ca^{2+} release from intracellular stores, which initiated local $[\text{Ca}^{2+}]_i$ transients or propagating Ca^{2+} waves [30]. Although the exact sequence of the events and their interplay have not been explained, the authors concluded that the primary effect of nsPEF was the formation of Ca^{2+} -permeable nanopores in the plasmalemma at the anodal pole of the cell. A recent study utilizing fast Ca^{2+} imaging in neuroblastoma cells showed both Ca^{2+} release from the ER and its entry from the outside after a single 600-ns pulse at 16 kV/cm [17]; in contrast to what was observed in myocytes with 4-ns pulses, the entry of external Ca^{2+} originated from the cathodic pole of the cell.

However, Vernier et al [31] reported that $[\text{Ca}^{2+}]_i$ increase evoked by ten 30-ns pulses (25 kV/cm) in Jurkat cells was not affected by the addition of 5 mM EGTA into the external medium. Among diverse Ca^{2+} blockers tested, only thapsigargin reduced the response to nsPEF, thereby suggesting that nsPEF released Ca^{2+} from the ER without affecting the cell plasma membrane. Another study in Jurkat cells [32] reported that 60-ns PEF (25–50 kV/

cm) triggered exclusively Ca^{2+} release from the ER, whereas the threshold for extracellular Ca^{2+} uptake was as high as 100 kV/cm. These findings are in stark contradiction with electrophysiological [11, 12, 33] and fluorescent microscopy data [34] that nanoporation of the plasma membrane by 60-ns pulses occurs already at 6–15 kV/cm.

In contrast to the uptake of relatively inert dyes like propidium or YO-PRO-1 and ions like Tl^+ , the entry of Ca^{2+} triggers active mechanisms aimed at both the reduction of $[\text{Ca}^{2+}]_i$ and active amplification of $[\text{Ca}^{2+}]_i$ signal. Such complex effects are difficult or impossible to discern when $[\text{Ca}^{2+}]_i$ changes are detected as a fold change to the initial fluorescence level [9, 17, 28–32] and can be better resolved by measuring the actual rather than relative change in $[\text{Ca}^{2+}]_i$.

Given that $[\text{Ca}^{2+}]_i$ changes (by either Ca^{2+} uptake or release from the ER) play the principal role in determining nsPEF bioeffects, and that nsPEF stimulation offers a unique opportunity for non-chemical mobilization of the internal Ca^{2+} , we performed a detailed analysis of nsPEF-triggered changes in $[\text{Ca}^{2+}]_i$ using fast ratiometric Ca^{2+} imaging with FURA-2 dye [35]. This method reliably measures nanomolar changes in $[\text{Ca}^{2+}]_i$ over time intervals of tens of milliseconds; combined with pharmacological testing, the ratiometric Ca^{2+} imaging constitutes a powerful and quantitative tool in the analysis of intracellular Ca^{2+} response. For most accurate interpretation of nsPEF effects, we used CHO cells which express few endogenous channels [36] and typically lack any voltage-gated channels. Below we demonstrate that even in CHO cells, nsPEF can stimulate both Ca^{2+} uptake from the outside and its release from the ER. Remarkably, the changes in $[\text{Ca}^{2+}]_i$ closely resemble cell responses to stimulation of Ca^{2+} pathway-coupled receptors, but can be elicited without any chemical agonists.

2. Materials and methods

2.1. Cell lines and propagation

Experiments were performed in CHO-K1 cells (Chinese hamster ovary). The cells were obtained from the American Type Culture Collection (ATCC, Manassas, VA) and propagated in Ham's F12K medium at 37 °C with 5% CO_2 in air. The medium also contained 10% FBS and 100 I.U./ml penicillin and 0.1 $\mu\text{g}/\text{ml}$ streptomycin. The media and its components were purchased from Mediatech Cellgro (Herndon, VA) except for serum (Atlanta Biologicals, Norcross, GA). For the passage immediately preceding experiments, cells were transferred onto "0" thickness glass coverslips, and the experiments were carried out 12–24 hours afterwards. Attached cells were irregularly shaped, with typical linear dimensions from 15 to 40 μm .

2.2. Reagents and solutions

Fura-2 pentapotassium salt, Fura-2/AM, Calcium Calibration Buffer Kit, and Pluronic F-127 (20% solution in DMSO) were purchased from Life Technologies (Grand Island, NY). Other chemicals were obtained from Sigma-Aldrich (St. Louis, MO).

During experiments, cells were continually perfused (0.5 ml/min) with a physiological solution containing (in mM): 140 NaCl, 5.4 KCl, 1.5 MgCl_2 , 2 CaCl_2 , 10 glucose, and 10 HEPES (pH 7.3, 300–310 mOsm/kg). For Ca^{2+} -free conditions, CaCl_2 was replaced with 2 mM Na-EGTA.

2.3. Exposure to nsPEF and modeling of the local electric field

The method of exposure to nsPEF was similar to what was described recently [25, 37], but the transmission line-based pulse generator was replaced with a Blumlein line-type circuit

with a 2-fold higher maximum voltage output (about 1 kV). This circuit was formed by two 50 Ohm coaxial cables (RG58) connected in series into a 100 Ohm pulse forming network. A 1 MOhm resistor was used to charge the pulse forming network, and the discharge was controlled by a high speed closing MOSFET switch (DE275-102N06A, IXYSRF, <4 ns rise time). The reason for using a 100 Ohm pulse forming network was to reduce the impact of the turn-on resistance of the MOSFET switch, so that tail-free, nearly rectangular pulses were generated. The pulses were delivered to a 200 Ohm load, which, in our case, included the resistance between a pair of tungsten rod electrodes (0.08 mm diameter) submerged into the physiological solution and one additional resistor for matching the overall resistance to 200 Ohm.

With the help of an MPC-200 robotic manipulator (Sutter, Novato, CA), the electrodes were positioned precisely at 30 μm above the coverslip surface so that selected cells were in the middle of the 0.15-mm gap between their tips. The electric field at the location of the cells was determined by a 3D simulation with a finite-element Maxwell equation solver Amaze 3D (Field Precision, Albuquerque, NM).

In this study, we used nsPEF of 60-ns duration at the E-field intensity from 3.7 to 30 kV/cm (0 kV/cm for sham exposure). nsPEF was triggered externally and synchronized with image acquisition and bath buffer exchanges by a TTL pulse protocol using Digidata 1440A board and Clampex v. 10.2 software (Molecular Devices, Sunnyvale, CA). When applying multiple pulses, they were delivered at a rate of 20Hz.

In most experiments, 4–8 cells were exposed to nsPEF together. The cells were located within about a 60 μm radius from the center point between the tips of nsPEF-delivering electrodes. The cells were randomly oriented with respect to each other and the electrodes; we did not notice any impact of cell orientation or size on the effect of nsPEF. Repetitive Ca^{2+} imaging started at least 1 min prior to nsPEF application, and continued for 5–10 min afterwards. Any group of cells was exposed to nsPEF only once. For statistical analysis, the experiments were repeated 3–10 times in different cell groups and on different coverslips. To compare several treatment conditions (e.g., the effects of different nsPEF amplitudes), these conditions were tested in a random sequence.

Numerical data were statistically analyzed using Origin 8.0 software package (Origin Lab, Northampton, MA). The thresholds E-field values were estimated by linear fitting of the experimental data.

2.4. Measurement of $[\text{Ca}^{2+}]_i$

Cells on coverslips were loaded with Fura-2/AM by incubation for 30 min in the physiological solution containing 5 μM of the dye and 0.05% of Pluronic F-127 (0.05%). The incubation was performed in the dark at room temperature (21 $^{\circ}\text{C}$).

The coverslips were washed in the physiological solution for at least 10 min and transferred into a glass-bottomed perfusion chamber (Warner Instruments, Hamden, CT) mounted on an IX71 inverted microscope (Olympus America, Center Valley, PA).

The dye was excited in 5-ms windows, alternatively at 340 and 380 nm, with a help of a fast wavelength switcher Lambda DG4 (Sutter Instruments, Novato, CA). We utilized an ET FURA2 filter set (Chroma Technology, Bellows Falls, VT) and a UApo/340 40 \times /0.9 objective (Olympus). Emission was measured at 510 nm (40 nm half bandwidth) using a C9100-02 EM CCD camera (Hamamatsu Photonics, Hamamatsu City, Japan). The image acquisition and on-line data analysis were accomplished with Metafluor v.7.5. (Molecular Devices)

Fura-2 emission ratio (R) at the two excitation wavelengths was calibrated against Ca^{2+} concentration using Calcium Calibration Buffer Kit and following the manufacturer's instructions. In brief, increasing the concentration of free Ca^{2+} ($[\text{Ca}^{2+}]_o$) shifts the maximum of Fura-2 excitation from 380 to 340 nm. R is linked to $[\text{Ca}^{2+}]_o$ by the following equation:

$$R = (R_{\max} - R_{\min}) / (1 + (\beta \times K_d) / [\text{Ca}^{2+}]_i) + R_{\min} \quad 1.1$$

where K_d is dissociation constant of Fura-2; R_{\min} and R_{\max} are the ratios of emission for two excitation wavelengths for Ca^{2+} -free and Ca^{2+} -saturated conditions, respectively; and β is the ration of emissions for Ca^{2+} -free and Ca^{2+} -saturated for excitation at 380 nm [35]. The values of R_{\min} , R_{\max} , and β were found from the experimental data directly. To determine K_d , we measured R in each of the calibration solutions and plotted R values against $[\text{Ca}^{2+}]_o$. K_d was obtained by fitting of R as a function of $[\text{Ca}^{2+}]_o$ using Origin 8.0 software.

For our setup, the calibration values were: $R_{\max}=4.0$; $R_{\min}=0.1$; $\beta=6.13$; and $K_d = 220$ nM. The concentration of free Ca^{2+} in cells ($[\text{Ca}^{2+}]_i$) was calculated according to [35] as:

$$[\text{Ca}^{2+}]_i = (R_{\max} - R) / (R - R_{\min}) \times K_d \times \beta \quad 1.2$$

All fluorescence ratios were calculated after subtraction of the background fluorescence. Calcium response traces presented in this paper were obtained by averaging individual traces from 15 or more cells. To maximize the signal-to-noise ratio and improve the sensitivity and accuracy of $[\text{Ca}^{2+}]_i$ measurements, individual traces were smoothed with a percentile filter utility of Origin 8.0. However, the smoothing procedure slightly distorted the traces, e.g., produced a false impression of a slow response onset in Figs. 5 and 6.

3. Results

3.1. nsPEF-induced $[\text{Ca}^{2+}]_i$ increase: Two distinct types of the response

In CHO cells bathed in the physiological solution with 2 mM Ca^{2+} , $[\text{Ca}^{2+}]_i$ was stable at about 100 nM. The experimental protocol included recording of the resting $[\text{Ca}^{2+}]_i$ for at least one minute prior to the administration of a single 60-ns pulse. Starting with a threshold of approximately 9 kV/cm, nsPEF caused an immediate increase in $[\text{Ca}^{2+}]_i$ proportionally to the pulse intensity. The increase lasted several minutes and was remarkably different for low (approximately 9 to 19 kV/cm) and high (> 19 kV/cm) nsPEF intensities (Fig. 1). For the lower intensities of nsPEF, $[\text{Ca}^{2+}]_i$ increased to no more than just 200–350 nM; the rise time and overall shape of the response were highly variable, often with little or no recovery to the resting value of 100 nM within 5 min of observation. For more intense nsPEF, most cells responded with $[\text{Ca}^{2+}]_i$ increase to as high as 1–3 μM within 10–50 s after the pulse, followed by a gradual return to the resting value over the next 2–3 min. When responses to low- and high-amplitude nsPEF were plotted on the same scale (Fig. 1B), they formed two distinctly different groups, thereby suggesting the involvement of different response mechanisms.

Within both these groups, the peak amplitude of $[\text{Ca}^{2+}]_i$ response (as measured within 1 min after nsPEF) grew linearly with nsPEF intensity, at the rate of 8 ± 1.4 nM per 1 kV/cm for E-field values under 19 kV/cm, and at 174 ± 12 nM per 1 kV/cm for E-field values exceeding 19 kV/cm. Thus, the dose-response curve displayed a sharp bend at about 19 kV/cm (Fig. 2A).

This bend was completely eliminated by pre-incubation of cells with thapsigargin (TG), a specific and irreversible blocker of Ca^{2+} -ATPase (SERCA) of the endoplasmic reticulum

(Fig. 2A). In intact cells, SERCA pumps Ca^{2+} from the cytosol to the lumen of the ER. Inhibition of this process with TG results in complete withdrawal of Ca^{2+} ions from ER into the cytoplasm, where the plasma membrane Ca^{2+} -ATPase (PMCA) and the sodium-calcium exchanger (NCX) pump them out of the cell [38]. These processes are manifested by a slow bell-shaped $[\text{Ca}^{2+}]_i$ change in response to perfusion with 100 nM TG (Fig 3A).

For experiments with nsPEF, 100 nM of TG were added to the extracellular buffer already at the start of loading the cells with Fura-2/AM, and were also present in the physiological solution afterwards. By this protocol, nsPEF was delivered after a minimum of 40 min of incubation with TG, which was more than adequate for complete depletion of Ca^{2+} from the ER (Fig. 3A). Noteworthy, depletion of the ER Ca^{2+} with TG can trigger capacitative Ca^{2+} entry from the outside [39, 40]. The rate of the capacitative entry varies among individual CHO cells, so we were able to select for nsPEF exposure only those cells which recovered to the resting $[\text{Ca}^{2+}]_i$ of about 100 nM (i.e., cells with minimum capacitative entry).

These cells responded to nsPEF with an abrupt rise of $[\text{Ca}^{2+}]_i$, followed by a smooth and relatively fast (1–2 min) return to the resting level (Fig. 3B). The late, random components of the response seen in Fig. 1A (11.2–18.7 kV/cm) were eliminated by TG, and thereby were likely a physiological response caused by a delayed Ca^{2+} release from ER. In contrast, the amplitude of the early response (within 1 min after nsPEF) to low-intensity nsPEF stimuli (<19 kV) was identical with or without TG and apparently was determined by Ca^{2+} entry from the outside (Fig 3C). Most importantly, TG fully eliminated the bend of the dose-response curve which remained linear at 13 ± 1.3 nM per 1 kV/cm up to the highest E-field tested (Fig. 2A).

Thus, $[\text{Ca}^{2+}]_i$ early response to low-intensity nsPEF was caused by Ca^{2+} entry from the outside and did not depend on the ER Ca^{2+} store. In contrast, the major amplification of the response when the E-field exceeded 19 kV/cm was fully dependent on Ca^{2+} release from the ER. To check if the intense nsPEF directly causes Ca^{2+} release from the intracellular stores, our next step was the analysis of $[\text{Ca}^{2+}]_i$ response in the absence of external Ca^{2+} .

3.2. nsPEF-induced intracellular Ca^{2+} release in a Ca^{2+} -free buffer

In these experiments, 2 mM Ca^{2+} in the extracellular buffer were replaced with 2 mM EGTA to remove any residual free Ca^{2+} . Under such conditions, the ER was the only appreciable source of $[\text{Ca}^{2+}]_i$ increase in response to nsPEF stimulation: When the ER store was depleted with TG, even a train of 4 pulses of the maximum intensity (30 kV/cm) caused no change in $[\text{Ca}^{2+}]_i$ (Fig. 4).

The removal of the external Ca^{2+} had a profound effect on the response to nsPEF. $[\text{Ca}^{2+}]_i$ increased rapidly (within seconds after the stimulus) and gradually returned to the resting value in 50–100 s (Fig. 5). The E-field threshold for Ca^{2+} response was at about 19 kV/cm (Fig. 2B); this value was twofold greater than the threshold in the presence of external Ca^{2+} (9kV/cm). Interestingly, the 19 kV/cm threshold matched the critical E-field value required for the amplification of Ca^{2+} response in the presence of external Ca^{2+} (Fig. 2). We do not know yet if this similarity was by coincidence only or pointed to some mechanistic connection.

Above the 19 kV/cm threshold, the amplitude of nsPEF-induced $[\text{Ca}^{2+}]_i$ transients increased linearly (at a rate of 5.6 ± 2 nM per 1 kV/cm) until reaching the critical E-field value of 30 kV/cm, where the response increased sharply. As a result, the dose-response curve showed similar bend as in the presence of external Ca^{2+} , but it was shifted from about 19 kV/cm to 26 kV/cm (Fig. 2B).

In actuality, the response to 30 kV/cm nsPEF was amplified in only about 50% of cells. Grouping separately the cells with “amplified” and “non-amplified” response has revealed distinct differences in the response kinetics (Fig. 6). The non-amplified response represented a single, fast transient that reached the peak of about 200 nM within 3–4 s after nsPEF (blue trace, n=34). The amplified response started the same way, but $[Ca^{2+}]_i$ exceeded 200 nM and was followed by a second high-amplitude rise (green trace, n=21). These two phases of the response were better discerned by differentiating the original traces and plotting $d[Ca^{2+}]_i/dt$ versus time (Fig. 6, bottom plots). Differentiated traces show that at 2 s after nsPEF, the rate of $[Ca^{2+}]_i$ rise ceased to decline and increased again in cells with amplified response, but continued to decline in cells with non-amplified response (Fig. 6, arrows). Thus, the second phase of the response started (or became detectable) at about 2 s after nsPEF, corresponding to $[Ca^{2+}]_i$ rise to approximately 300 nM (Fig. 6, right panels). In retrospect, these two phases of the response could also be discerned in amplified $[Ca^{2+}]_i$ responses with 2 mM Ca^{2+} outside.

Summarizing the above observations, we conclude that it was not the nsPEF intensity *per se* responsible for the amplified response. Instead, nsPEF just triggered Ca^{2+} influx from the outside and/or Ca^{2+} efflux from the ER, supposedly by a direct electropermeabilization of the cell plasma membrane and ER membranes. Once the $[Ca^{2+}]_i$ reached 200–300 nM (or 100–200 nM above the basal level of 100 nM), and regardless of how this critical level was reached, the Ca^{2+} response was biologically amplified via a Ca^{2+} -induced Ca^{2+} release (CICR) positive feedback mechanism [23, 24].

CICR is caused or facilitated by Ca^{2+} -induced activation of ER calcium channels, which, in most cell types, are represented by inositol trisphosphate receptors (IP₃R) and ryanodine receptors (RyR). These receptors, when activated by increased $[Ca^{2+}]_i$, enable additional Ca^{2+} release from the ER, leading to further activation of the receptors and profound amplification of the initially modest $[Ca^{2+}]_i$ response. The subsequent experiments established that the amplified $[Ca^{2+}]_i$ response to nsPEF was indeed a secondary physiological response, namely the IP₃R-mediated CICR.

3.3. Blocking of IP₃R abolishes the amplification of $[Ca^{2+}]_i$ response to nsPEF

Exposure of CHO cells to a RyR agonist caffeine (up to 40 mM) or RyR blocker dantrolene (50 μM) did not change the resting $[Ca^{2+}]_i$ or the response to nsPEF (data not shown). This result was expected and consistent with other studies which reported no evidence of endogenous RyR expression in CHO cells [41, 42]. Therefore, we focused on the role of IP₃R, which is abundantly expressed and well-studied in CHO cells [43–46].

We found that the addition of 50 μM of an IP₃R blocker 2-aminoethoxydiphenyl borate (2-APB) to the perfusion buffer a few minutes before nsPEF prevented the amplification of $[Ca^{2+}]_i$ response, but had no effect on the amplitude of “non-amplified” $[Ca^{2+}]_i$ transients at lower nsPEF intensities. This effect of 2-APB has been shown both in the presence of external Ca^{2+} (Fig. 2C) and its absence (Figs. 2B and 7). In the presence of external Ca^{2+} , blockage of IP₃R with 2-APB had essentially the same effect as the depletion of ER Ca^{2+} with TG (Fig. 2, A and C).

Although this similarity was consistent with CICR mechanism, it could also be indicative of a non-specific inhibition of SERCA by 2-APB; the possibility of this side effect of 2-APB was noted elsewhere [47, 48]. If SERCA was indeed inhibited by 2-APB, this would be manifested by the characteristic Ca^{2+} efflux from the ER, similar to the effect of TG. However, we observed no sign of Ca^{2+} efflux after several minutes of perfusion with 2-APB, whereas the amplification of the response to nsPEF was inhibited to the same extent as after ER depletion with TG (Fig. 7). This result is corroborated by data in Fig. 2B, which

shows that the “non-amplified” Ca^{2+} efflux from ER after exposure to 26 kV/cm nsPEF was not affected by 2-APB (if 2-APB caused Ca^{2+} leakage from the ER, the response to nsPEF would be diminished)

Thus, blockage of IP_3R prevented the amplification of $[\text{Ca}^{2+}]_i$ signal by CICR, even though the ER Ca^{2+} store remained untouched.

4. Discussion

Even in a relatively simple mammalian cell model (CHO cells), nsPEF produced complex effects that involved Ca^{2+} influx through permeabilized plasma membrane, Ca^{2+} efflux from the ER store, and physiological amplification of the Ca^{2+} signal by activation of IP_3R in CICR pathway. By combining the ratiometric Ca^{2+} imaging with pharmacological agents, varying the composition of the bath buffer, and testing the response for a wide range of nsPEF amplitudes, we were able to isolate each of the response mechanisms, quantify their sensitivity to nsPEF, and contribution to the overall response.

Cell plasma membrane was most sensitive to 60-ns electric pulses, with the threshold at about 9 kV/cm. This result matches well with the 6 kV/cm threshold for nanopore formation as detected by patch clamp in CHO cells [33]. Likewise, a single 60-ns pulse of 14 kV/cm elicited TI^+ entry into the cell [34]; the threshold for this effect was at or below 11 kV/cm (A. Pakhomov, unpublished data). In HL60 cells, the supposed capacitative Ca^{2+} entry (which, as we now believe, was actually the entry through nanoelectropores) occurred at a somewhat lower but still close E-field level of 6.4 kV/cm [14].

In the absence of external Ca^{2+} , the threshold for Ca^{2+} efflux from the ER was about 2-fold higher, at about 19 kV/cm. Hence, any $[\text{Ca}^{2+}]_i$ response to nsPEF weaker than 19 kV/cm was primarily determined by the external Ca^{2+} entry (although the response might include late secondary components dependent on the ER, Figs. 1A and 3C). These data are also consistent with observations in HL60 cells (one 60-ns pulse at 15 kV/cm elevated $[\text{Ca}^{2+}]_i$ in the absence of external Ca^{2+}); the authors did not look specifically for the threshold of the effect [14].

Both the entry of Ca^{2+} from the outside and its efflux from the ER (except late components of the response) are, most likely, caused directly by permeabilization of these membranous structures by nsPEF. As long as $[\text{Ca}^{2+}]_i$ does not exceed the critical value of 200–300 nM, the nsPEF-induced $[\text{Ca}^{2+}]_i$ rise appears inconsequential and does not even seem to trigger $[\text{Ca}^{2+}]_i$ removal, at least within the studied time span. Then, the ratio of Ca^{2+} efflux from ER to its entry from the outside can serve as an accurate index of nsPEF efficacy to permeabilize internal membranes versus the plasma membrane. If theoretical predictions of nsPEF ability to cause intracellular poration are correct, reducing nsPEF duration should increase this ratio, while using longer pulses may bring it to zero. The experiments intended to test this hypothesis by comparing 10-, 60-, and 600-ns pulses are already in progress and will be reported soon.

While it may be surprising that pulses as short as 4 and 5 ns did not trigger Ca^{2+} efflux from the ER in either myocytes or adrenal chromaffin cells [28–30], it is possible that all tested pulse amplitudes were below the threshold for either plasma membrane or ER permeabilization. Indeed, to the extent it was studied, Ca^{2+} entry in chromaffin cells was determined mostly or completely by opening of voltage-gated Ca^{2+} channels. These channels are activated by membrane depolarization by 30–50 mV, whereas the transmembrane potential required for electroporation is about an order of magnitude greater [1, 2, 8]. Hence, one may infer that in excitable cells the membrane electroporation will always be accompanied by opening of voltage-sensitive channels, unless they are

deliberately blocked or inactivated. Furthermore, opening of ion channels will effectively increase the membrane conductance and may reduce the efficiency of forthcoming pulses in high-rate nsPEF trains.

In CHO cells, reaching the critical $[Ca^{2+}]_i$ of 200–300 nM triggered a dramatic amplification of the nsPEF effect by CICR. Importantly, this biological response far exceeded the effect of nsPEF *per se*, and it no longer mattered whether the initial “kindling” occurred by Ca^{2+} uptake from the outside or efflux from the ER. Perhaps it was the activation of CICR that prevented Scarlett et al. [32] from observing the difference in nsPEF effects with and without external Ca^{2+} (one 60-ns pulse at 25 or 50 kV/cm, Jurkat cells). By not seeing this difference, the authors concluded that the response was elicited exclusively by ER electroperoration, which disagrees with all other relevant data on nanoporation [3, 10–12, 14, 25–27, 33, 34]. However, other effects reported in that paper, including “spontaneous” Ca^{2+} oscillations and qualitative change of Ca^{2+} response at 100 kV/cm, still require a better explanation.

It is important to emphasize that the maximum effect from nsPEF itself (i.e., when CICR was blocked) was rather modest. Under such conditions, $[Ca^{2+}]_i$ increased to no more than 400–500 nM (Fig. 7) followed by gradual recovery. Hence, the electroperorative damage to membranes from nsPEF was limited and contained, and $[Ca^{2+}]_i$ changes from electroperoration remained well under physiological limits: they were 5–10 times smaller than physiological $[Ca^{2+}]_i$ transients produced by CICR.

Overall, electroperoration by nsPEF mimicked Ca^{2+} signaling that would normally originate from the activation of membrane receptors or channels, but did not require their activation and therefore did not depend on their state, refractoriness, inactivation, etc. Taken the limited and transient nature of the membrane disruption, nsPEF stimulation may be a unique approach for non-chemical activation of Ca^{2+} signaling in various types of cells, including cells that have no voltage-sensitive membrane channels. Even in excitable cells which do have such channels, nsPEF-induced signals will overcome limitations imposed by the channels’ activation and inactivation properties or modulation through various pathways. It has already been proposed earlier to employ nsPEF for heart pacing [16] and stimulation of catecholamine release [25, 33], but better understanding of nsPEF effects may open the way for numerous other applications.

Acknowledgments

The study was supported by R01CA125482 from the National Cancer Institute and R01GM088303 from the National Institute of General Medical Sciences (AGP).

Abbreviations

2-APB	2-aminoethoxydiphenyl borate
CICR	Ca^{2+} -induced Ca^{2+} -release
$[Ca^{2+}]_i$	intracellular concentration of free Ca^{2+} ions
$[Ca^{2+}]_o$	extracellular concentration of free Ca^{2+} ions
DMSO	dimethylsulfoxide
EGTA	ethylene glycol tetraacetic acid
ER	endoplasmic reticulum
FBS	fetal bovine serum

IP₃R	inositol-1,4,5- trisphosphate receptor
K_d	dissociation constant
NCX	sodium-calcium exchanger
nsPEF	nanosecond pulsed electric field
PMCA	plasma membrane Ca ²⁺ ATPase
RyR	ryanodine receptor
SERCA	sarco/endoplasmic reticulum Ca ²⁺ -ATPase
TG	thapsigargin

References

1. Neumann, E.; Sowers, AE.; Jordan, CA. *Electroporation and Electrofusion in Cell Biology*. Plenum; New York: 1989.
2. Zimmermann, U.; Neil, GA. *Electromanipulation of cells*. CRC Press; Boca Raton: 1996.
3. Pakhomov, AG.; Miklavcic, D.; Markov, MS. *Advanced Electroporation Techniques in Biology in Medicine*. CRC Press; Boca Raton: 2010. p. 528
4. Rubinsky, B., editor. *Series in Biomedical Engineering*. Springer-Verlag; Berlin Heidelberg: 2010. Irreversible Electroporation.
5. Schoenbach KH, Beebe SJ, Buescher ES. Intracellular effect of ultrashort electrical pulses. *Bioelectromagnetics*. 2001; 22:440–448. [PubMed: 11536285]
6. Schoenbach, KH. Bioelectric effect of intense nanosecond pulses. In: Pakhomov, AG.; Miklavcic, D.; Markov, MS., editors. *Advanced Electroporation Techniques in Biology in Medicine*. CRC Press; Boca Raton: 2010. p. 19-50.
7. Gowrishankar TR, Weaver JC. Electrical behavior and pore accumulation in a multicellular model for conventional and supra-electroporation. *Biochem Biophys Res Commun*. 2006; 349:643–653. [PubMed: 16959217]
8. Kotnik T, Miklavcic D. Theoretical evaluation of voltage inducement on internal membranes of biological cells exposed to electric fields. *Biophys J*. 2006; 90:480–491. [PubMed: 16239325]
9. Craviso GL, Choe S, Chatterjee P, Chatterjee I, Vernier PT. Nanosecond electric pulses: a novel stimulus for triggering Ca²⁺ influx into chromaffin cells via voltage-gated Ca²⁺ channels. *Cell Mol Neurobiol*. 2010; 30:1259–1265. [PubMed: 21080060]
10. Vernier PT, Sun Y, Gundersen MA. Nanoelectropulse-driven membrane perturbation and small molecule permeabilization. *BMC Cell Biol*. 2006; 7:37. [PubMed: 17052354]
11. Pakhomov AG, Kolb JF, White JA, Joshi RP, Xiao S, Schoenbach KH. Long-lasting plasma membrane permeabilization in mammalian cells by nanosecond pulsed electric field (nsPEF). *Bioelectromagnetics*. 2007; 28:655–663. [PubMed: 17654532]
12. Pakhomov AG, Shevin R, White JA, Kolb JF, Pakhomova ON, Joshi RP, Schoenbach KH. Membrane permeabilization and cell damage by ultrashort electric field shocks. *Arch Biochem Biophys*. 2007; 465:109–118. [PubMed: 17555703]
13. Frey W, White JA, Price RO, Blackmore PF, Joshi RP, Nuccitelli R, Beebe SJ, Schoenbach KH, Kolb JF. Plasma membrane voltage changes during nanosecond pulsed electric field exposure. *Biophys J*. 2006; 90:3608–3615. [PubMed: 16513782]
14. White JA, Blackmore PF, Schoenbach KH, Beebe SJ. Stimulation of capacitative calcium entry in HL-60 cells by nanosecond pulsed electric fields. *J Biol Chem*. 2004; 279:22964–22972. [PubMed: 15026420]
15. Beebe SJ, Fox PM, Rec LJ, Willis EL, Schoenbach KH. Nanosecond, high-intensity pulsed electric fields induce apoptosis in human cells. *Faseb J*. 2003; 17:1493–1495. [PubMed: 12824299]

16. Napotnik TB, Wu YH, Gundersen MA, Miklavcic D, Vernier PT. Nanosecond electric pulses cause mitochondrial membrane permeabilization in Jurkat cells. *Bioelectromagnetics*. 2012; 33:257–264. [PubMed: 21953203]
17. Beier HT, Roth CC, Tolstykh GP, Ibey BL. Resolving the spatial kinetics of electric pulse-induced ion release. *Biochem Biophys Res Commun*. 2012; 423:863–866. [PubMed: 22713455]
18. Catterall WA. Structure and regulation of voltage-gated Ca^{2+} channels. *Annu Rev Cell Dev Biol*. 2000; 16:521–555. [PubMed: 11031246]
19. Kawamoto EM, Vivar C, Camandola S. Physiology and pathology of calcium signaling in the brain. *Frontiers in pharmacology*. 2012; 3:61. [PubMed: 22518105]
20. Partridge LD, Muller TH, Swandulla D. Calcium-activated non-selective channels in the nervous system. *Brain Research Reviews*. 1994; 19:319–325. [PubMed: 7820135]
21. Roberts-Crowley ML, Mitra-Ganguli T, Liu L, Rittenhouse AR. Regulation of voltage-gated Ca^{2+} channels by lipids. *Cell Calcium*. 2009; 45:589–601. [PubMed: 19419761]
22. Tapia R, Velasco I. Ruthenium red as a tool to study calcium channels, neuronal death and the function of neural pathways. *Neurochemistry International*. 1997; 30:137–147. [PubMed: 9017661]
23. Bootman MD, Berridge MJ, Roderick HL. Calcium signalling: more messengers, more channels, more complexity. *Curr Biol*. 2002; 12:R563–565. [PubMed: 12194839]
24. Roderick HL, Berridge MJ, Bootman MD. Calcium-induced calcium release. *Curr Biol*. 2003; 13:R425. [PubMed: 12781146]
25. Bowman AM, Nesin OM, Pakhomova ON, Pakhomov AG. Analysis of plasma membrane integrity by fluorescent detection of Tl^{+} uptake. *J Membr Biol*. 2010; 236:15–26. [PubMed: 20623351]
26. Nesin OM, Pakhomova ON, Xiao S, Pakhomov AG. Manipulation of cell volume and membrane pore comparison following single cell permeabilization with 60- and 600-ns electric pulses. *Biochim Biophys Acta*. 2011; 1808:792–801. [PubMed: 21182825]
27. Pakhomov, AG.; Pakhomova, ON. Nanopores: A distinct transmembrane passageway in electroporated cells. In: Pakhomov, AG.; Miklavcic, D.; Markov, MS., editors. *Advanced Electroporation Techniques in Biology in Medicine*. CRC Press; Boca Raton: 2010. p. 178-194.
28. Vernier PT, Sun Y, Chen MT, Gundersen MA, Craviso GL. Nanosecond electric pulse-induced calcium entry into chromaffin cells. *Bioelectrochemistry*. 2008; 73:1–4. [PubMed: 18407807]
29. Craviso GL, Choe S, Chatterjee I, Vernier PT. Modulation of intracellular Ca^{2+} levels in chromaffin cells by nanoelectropulses. *Bioelectrochemistry*. 2012; 87:244–252. [PubMed: 22197468]
30. Wang S, Chen J, Chen MT, Vernier PT, Gundersen MA, Valderrabano M. Cardiac myocyte excitation by ultrashort high-field pulses. *Biophys J*. 2009; 96:1640–1648. [PubMed: 19217879]
31. Vernier PT, Sun Y, Marcu L, Salem S, Craft CM, Gundersen MA. Calcium bursts induced by nanosecond electric pulses. *Biochemical and Biophysical Research Communications*. 2003; 310:286–295. [PubMed: 14521908]
32. Scarlett SS, White JA, Blackmore PF, Schoenbach KH, Kolb JF. Regulation of intracellular calcium concentration by nanosecond pulsed electric fields. *Biochim Biophys Acta*. 2009; 1788:1168–1175. [PubMed: 19230822]
33. Ibey BL, Xiao S, Schoenbach KH, Murphy MR, Pakhomov AG. Plasma membrane permeabilization by 60- and 600-ns electric pulses is determined by the absorbed dose. *Bioelectromagnetics*. 2009; 30:92–99. [PubMed: 18839412]
34. Ibey BL, Mixon DG, Payne JA, Bowman A, Sickendick K, Wilmink GJ, Roach WP, Pakhomov AG. Plasma membrane permeabilization by trains of ultrashort electric pulses. *Bioelectrochemistry*. 2010; 79:114–121. [PubMed: 20171148]
35. Grynkiewicz G, Poenie M, Tsien RY. A new generation of Ca^{2+} indicators with greatly improved fluorescence properties. *J Biol Chem*. 1985; 260:3440–3450. [PubMed: 3838314]
36. Gamper N, Stockand JD, Shapiro MS. The use of Chinese hamster ovary (CHO) cells in the study of ion channels. *Journal of pharmacological and toxicological methods*. 2005; 51:177–185. [PubMed: 15862463]
37. Pakhomova ON, Gregory BW, Khorokhorina VA, Bowman AM, Xiao S, Pakhomov AG. Electroporation-induced electrosensitization. *PloS one*. 2011; 6:e17100. [PubMed: 21347394]

38. Chen L, Koh DS, Hille B. Dynamics of calcium clearance in mouse pancreatic beta-cells. *Diabetes*. 2003; 52:1723–1731. [PubMed: 12829639]
39. Berridge MJ. Capacitative calcium entry. *Biochem J*. 1995; 312(Pt 1):1–11. [PubMed: 7492298]
40. Putney JW Jr. A model for receptor-regulated calcium entry. *Cell Calcium*. 1986; 7:1–12. [PubMed: 2420465]
41. Pan Z, Hirata Y, Nagaraj RY, Zhao J, Nishi M, Hayek SM, Bhat MB, Takeshima H, Ma J. Co-expression of MG29 and ryanodine receptor leads to apoptotic cell death: effect mediated by intracellular Ca^{2+} release. *J Biol Chem*. 2004; 279:19387–19390. [PubMed: 15039443]
42. Bhat MB, Zhao J, Zang W, Balke CW, Takeshima H, Wier WG, Ma J. Caffeine-induced release of intracellular Ca^{2+} from Chinese hamster ovary cells expressing skeletal muscle ryanodine receptor. Effects on full-length and carboxyl-terminal portion of Ca^{2+} release channels. *J Gen Physiol*. 1997; 110:749–762. [PubMed: 9382901]
43. Pan Z, Damron D, Nieminen AL, Bhat MB, Ma J. Depletion of intracellular Ca^{2+} by caffeine and ryanodine induces apoptosis of chinese hamster ovary cells transfected with ryanodine receptor. *J Biol Chem*. 2000; 275:19978–19984. [PubMed: 10764805]
44. Bhanumathy CD, Nakao SK, Joseph SK. Mechanism of proteasomal degradation of inositol trisphosphate receptors in CHO-K1 cells. *J Biol Chem*. 2006; 281:3722–3730. [PubMed: 16316991]
45. Nucifora FC Jr, Sharp AH, Milgram SL, Ross CA. Inositol 1,4,5-trisphosphate receptors in endocrine cells: localization and association in hetero- and homotetramers. *Molecular biology of the cell*. 1996; 7:949–960. [PubMed: 8817000]
46. Khan MT, Wagner L 2nd, Yule DI, Bhanumathy C, Joseph SK. Akt kinase phosphorylation of inositol 1,4,5-trisphosphate receptors. *J Biol Chem*. 2006; 281:3731–3737. [PubMed: 16332683]
47. Peppiatt CM, Collins TJ, Mackenzie L, Conway SJ, Holmes AB, Bootman MD, Berridge MJ, Seo JT, Roderick HL. 2-Aminoethoxydiphenyl borate (2-APB) antagonises inositol 1,4,5-trisphosphate-induced calcium release, inhibits calcium pumps and has a use-dependent and slowly reversible action on store-operated calcium entry channels. *Cell Calcium*. 2003; 34:97–108. [PubMed: 12767897]
48. Missiaen L, Callewaert G, De Smedt H, Parys JB. 2-Aminoethoxydiphenyl borate affects the inositol 1,4,5-trisphosphate receptor, the intracellular Ca^{2+} pump and the non-specific Ca^{2+} leak from the non-mitochondrial Ca^{2+} stores in permeabilized A7r5 cells. *Cell Calcium*. 2001; 29:111–116. [PubMed: 11162848]

Highlights

- Effects of 60 ns PEF on $[Ca^{2+}]_i$ were studied using fast measurements with Fura-2.
- nsPEF induced Ca^{2+} uptake via plasma membrane and Ca^{2+} efflux from ER.
- nsPEF of higher amplitudes triggered amplification of Ca^{2+} rise via CICR mechanism.
- Blocking of IP_3R abolished the amplification of Ca^{2+} response to nsPEF.

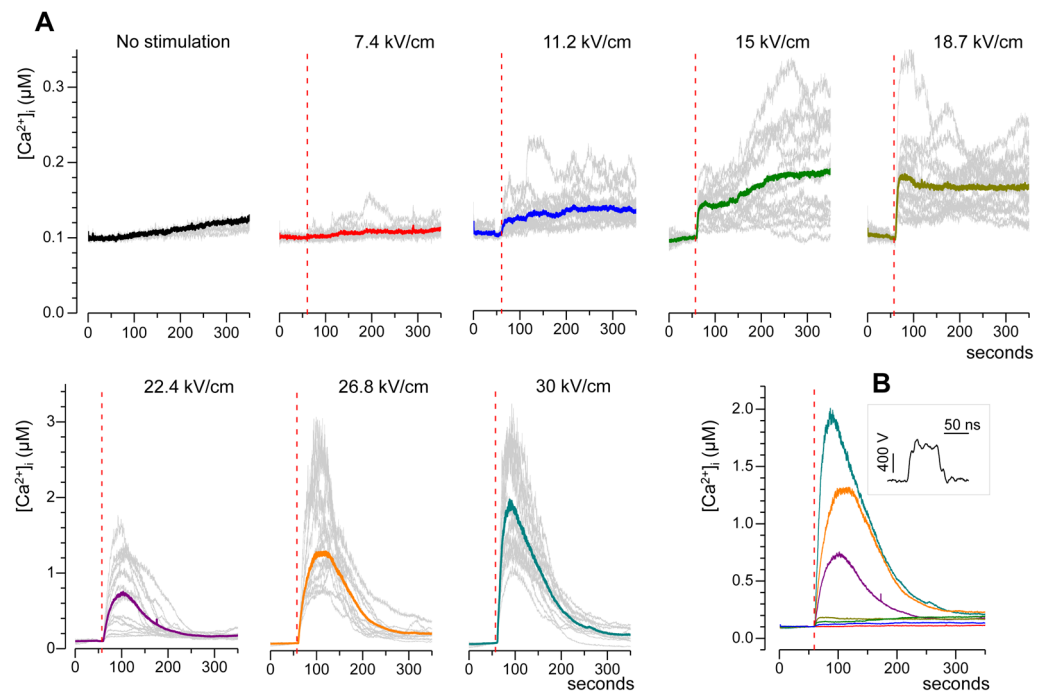


Fig. 1. Calcium transients evoked by a single 60-ns electric pulse in CHO cells. A: Typical responses as evoked by nsPEF at different pulse amplitudes (kV/cm). Cells were bathed in a physiological solution containing 2 mM Ca^{2+} . Shown are representative traces of the response in selected individual cells (gray lines, 15 cells per plot) and their average (color lines). NsPEF was delivered at 60 s into the experiment (vertical dashed lines). Note different vertical scales for panels in the top and bottom rows. B: The averaged traces from A plotted on the same scale for better comparison. The inset shows a representative waveform of a 60-ns pulse at the maximum output of the pulse generator.

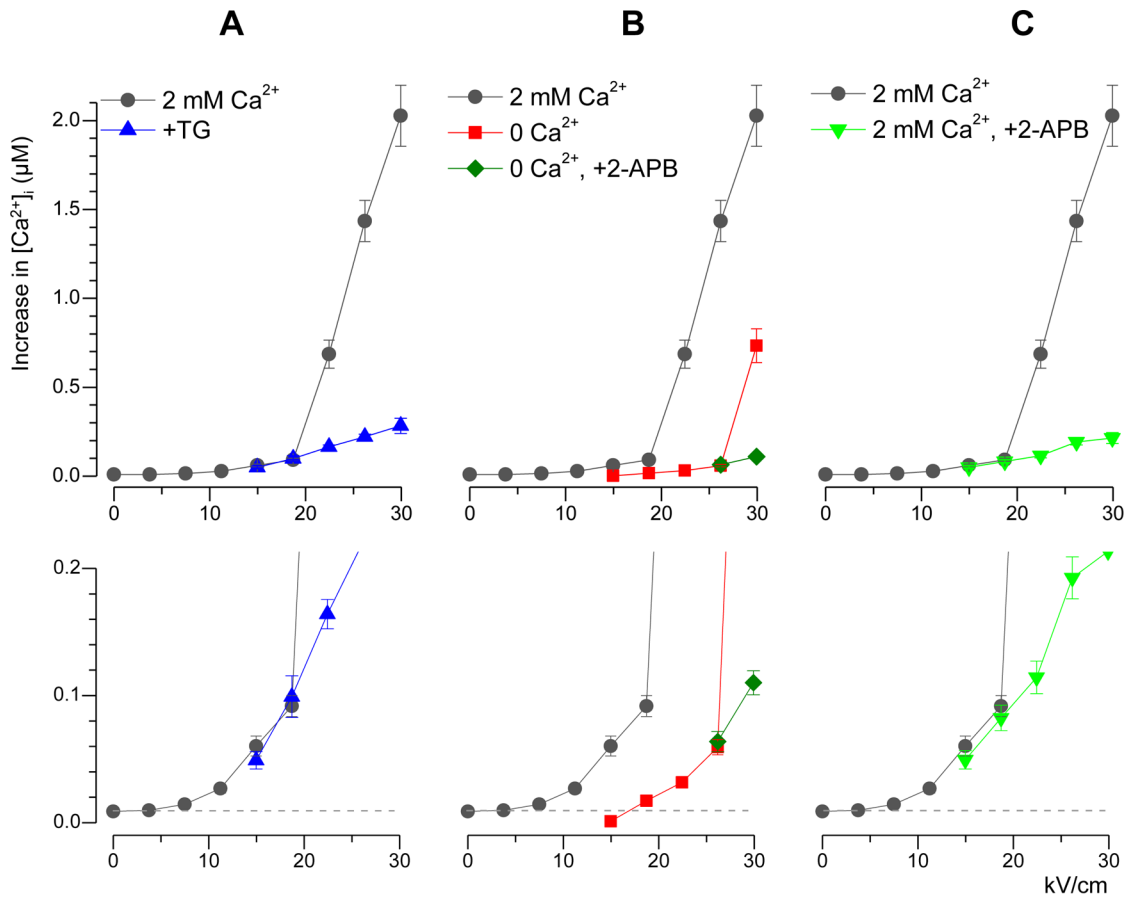


Fig. 2.

Mean amplitude of nsPEF-evoked calcium transients (μM) as a function of the stimulus intensity (kV/cm) under different experimental conditions. The amplitude was measured as a maximum reached within 1 min after nsPEF application. Mean \pm s.e.; $n=10-15$ for subthreshold E-field levels, and up to 50–60 elsewhere. Plots in the bottom row show the same data as above on an expanded vertical scale. In all panels, the data for 2 mM extracellular Ca^{2+} and no drug are shown as a control (black circles). Note amplification of the response at the E-field over 19 kV/cm . A: 100 nM thapsigargin (TG) did not change the response at low-intensity nsPEF, but abolished the amplification of response. B: Increased threshold and reduced amplitude of Ca^{2+} transients in the absence of external Ca^{2+} . Amplification of the response was observed only at 30 kV/cm and was abolished by 2-APB (50 μM). C: Same effect as in panel A but produced by 50 μM of 2-APB in the presence of 2 mM Ca^{2+} in the bath.

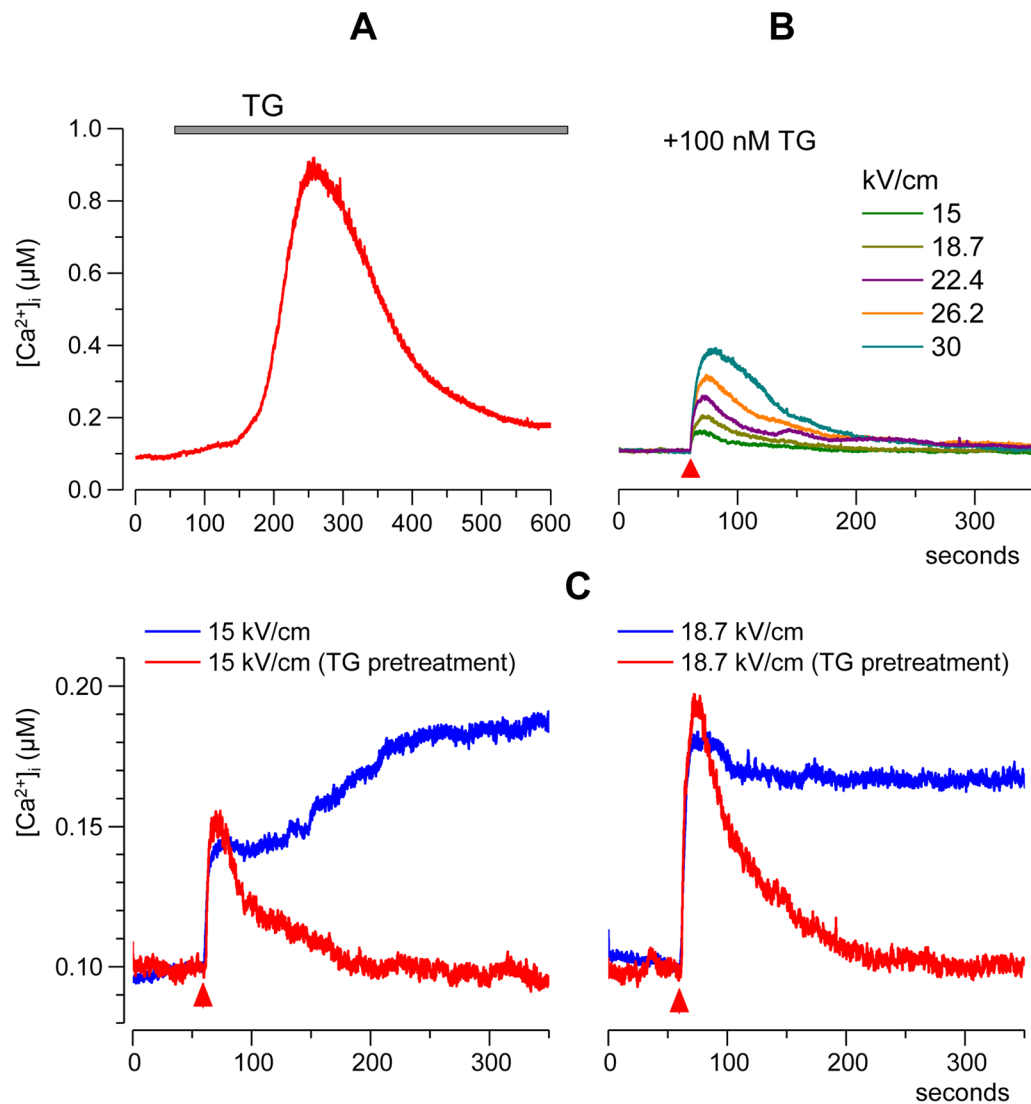


Fig. 3. Calcium response to incubation with 100 nM thapsigargin (A) and nsPEF-induced Ca^{2+} transients in thapsigargin-treated cells (B, C). Each trace is an averaged response from 15 cells. In A, TG was applied from 1 min till the end of the experiment. In B, cells were incubated with TG for a minimum of 40 min prior to nsPEF stimulation (red triangle; one 60-ns pulse of indicated intensity). Panel C illustrates the inhibition of late components of nsPEF-induced Ca^{2+} response by thapsigargin (TG). Note that the E-field intensity was below the 19 kV/cm threshold for immediate activation of Ca^{2+} -induced Ca^{2+} release. See subsection 3.1 for more detail.

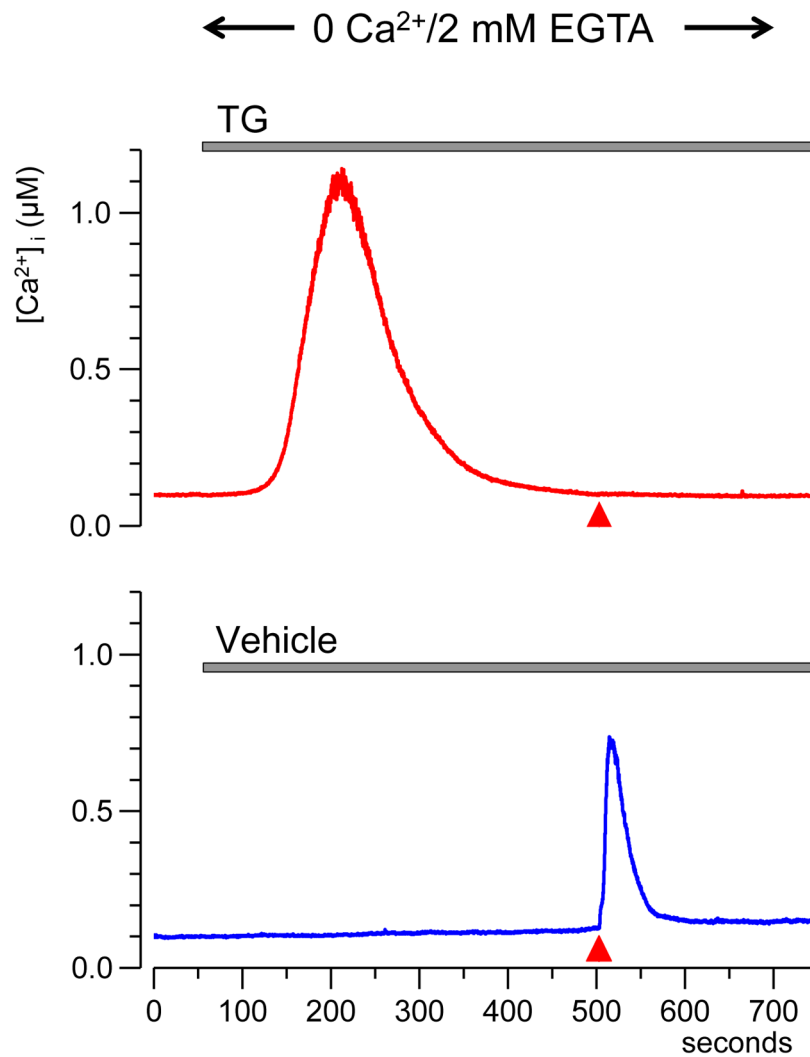


Fig. 4. Depletion of the endoplasmic reticulum Ca²⁺ store with thapsigargin (TG) blocks the response to nsPEF in a Ca²⁺-free medium. Top: perfusion with 100 nM TG (gray line) caused slow Ca²⁺ release from ER. After [Ca²⁺]_i return to the base level, even intense nsPEF stimulation (4 pulses at 30 kV/cm, red triangle) caused no response. Bottom: the response in control cells perfused with vehicle. Traces are the average from 15 cells.

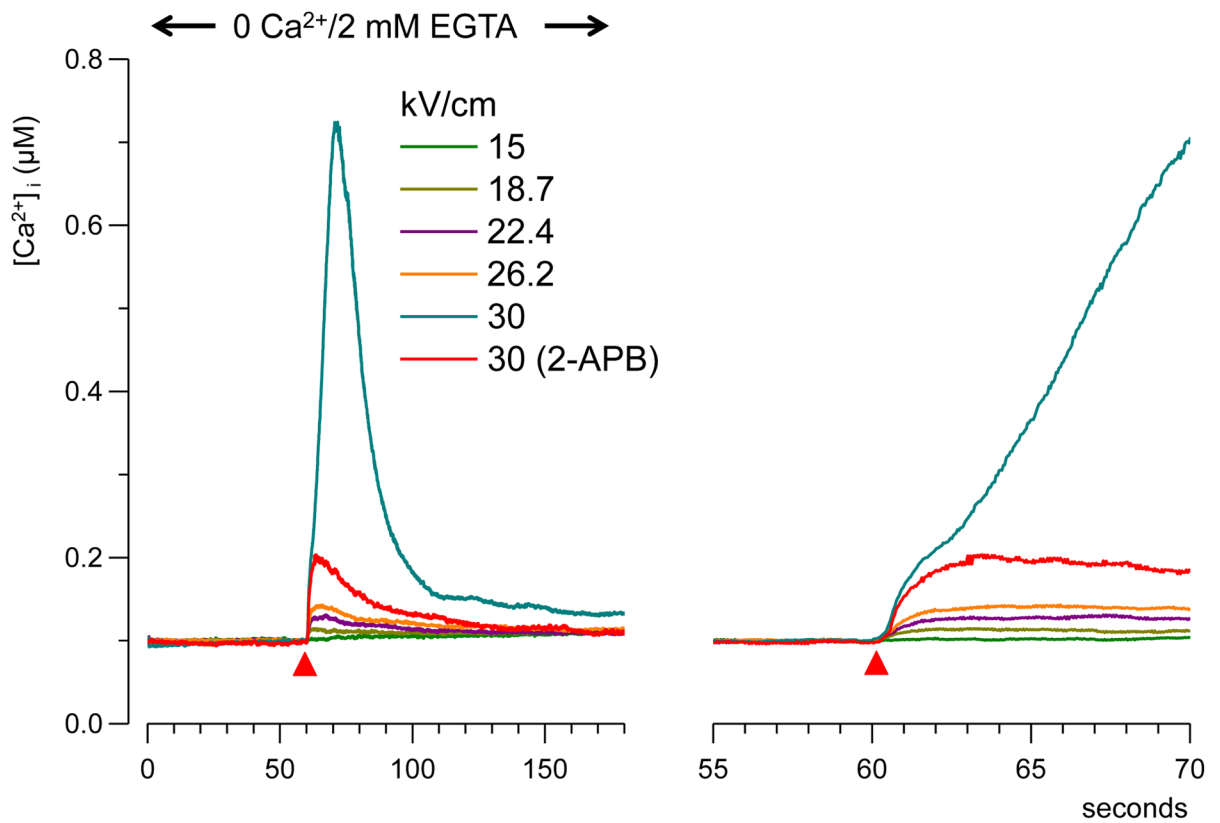


Fig. 5. NsPEF-evoked Ca^{2+} -transients in a Ca^{2+} -free medium. Cells were perfused for 3 min with $0 \text{ Ca}^{2+}/2 \text{ mM EGTA}$ physiological solution before the nsPEF stimulation. The right panel shows the onset of the transients on a faster time scale. Red triangles indicate the time of nsPEF application. Each trace is the average of at least 15 cells. At 30 kV/cm , $[\text{Ca}^{2+}]_i$ increase occurred in two steps, and the second step could be abolished with 2-APB. See subsection 3.2 and Fig. 6 for more detail.

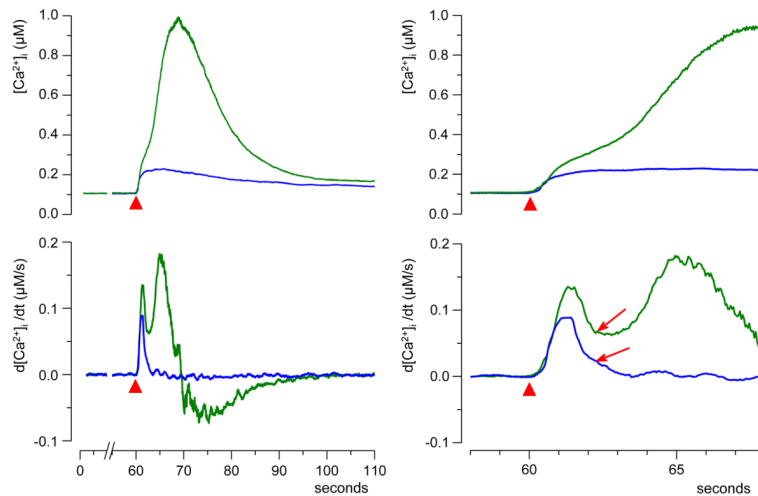


Fig. 6.

Two phases of the rising edge in “amplified” calcium transients. Top: Transients evoked by a single 60-ns pulse at 30 kV/cm (red triangle) in a Ca^{2+} -free medium. Left and right panels: same traces on a different time scale. All cells were separated in two distinct groups based on the amplitude of the transient (30 cells per group). Note the inflection on the rising edge of the high-amplitude (“amplified”) transient (arrow), and lack thereof for the low-amplitude one. The two phases of $[\text{Ca}^{2+}]_i$ increase can be discerned better in the differentiated traces (bottom). See subsection 3.2 for more detail.

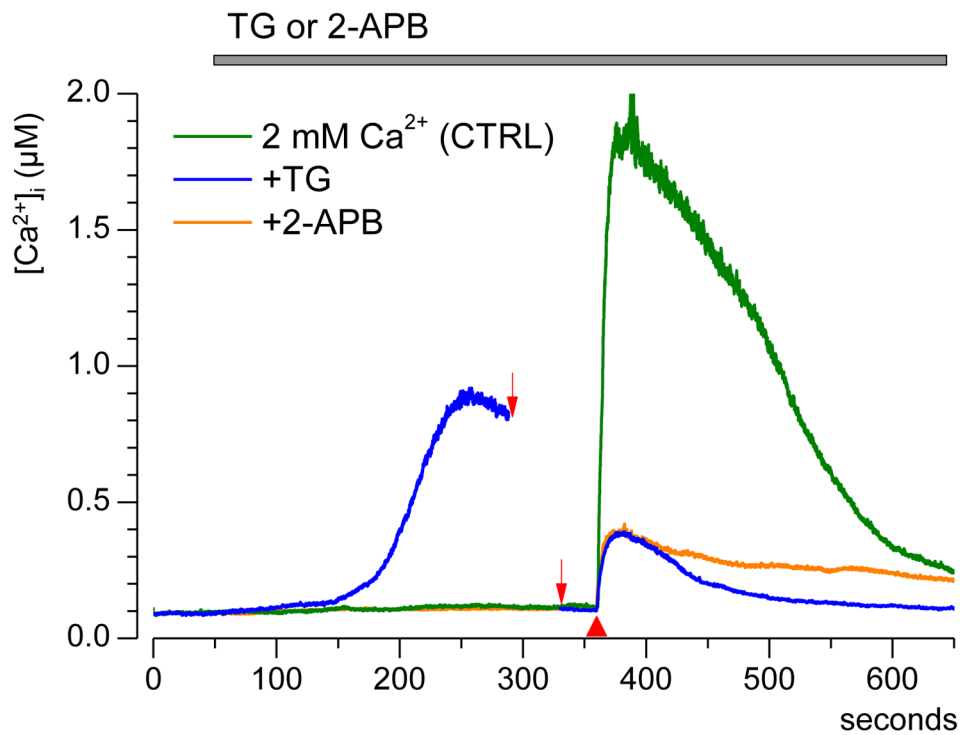


Fig. 7. IP₃R blocker 2-APB attenuates the nsPEF-induced Ca²⁺ transient without affecting the ER Ca²⁺ storage. Cells were stimulated by a single 60-ns pulse at 30 kV/cm (red triangle) after perfusion with either thapsigargin (TG), or 2-APB, or vehicle (control). Each trace is the average from 15 cells. The experiments with TG actually took longer to allow for the restoration of the basal [Ca²⁺]_i level; the omitted time interval between two arrows is 4.5 min. Although 2-APB and TG engaged different mechanisms to block Ca²⁺-induced Ca²⁺ release, both the drugs attenuated the response to nsPEF to the same extent.